Scientific
Research

Characterisation of Landscape with Forest Fragmentation Dynamics

T. V. Ramachandra, Uttam Kumar

Energy & Wetlands Research Group, *Centre for Ecological Sciences,*
Indian Institute of Science, Bangalore, India
E-mail: {*cestvr, energy, uttam*}*@ces.iisc.ernet.in*

Abstract

Land cover (LC) and land use (LU) dynamics induced by human and natural processes play a major role in global as well as regional patterns of landscapes influencing biodiversity, hydrology, ecology and climate. Changes in LC features resulting in forest fragmentations have posed direct threats to biodiversity, endangering the sustainability of ecological goods and services. Habitat fragmentation is of added concern as the residual spatial patterns mitigate or exacerbate edge effects. LU dynamics are obtained by classifying temporal remotely sensed satellite imagery of different spatial and spectral resolutions. This paper reviews five different image classification algorithms using spatio-temporal data of a temperate watershed in Himachal Pradesh, India. Gaussian Maximum Likelihood classifier was found to be apt for analysing spatial pattern at regional scale based on accuracy assessment through error matrix and ROC (receiver operating characteristic) curves. The LU information thus derived was then used to assess spatial changes from temporal data using principal component analysis and correspondence analysis based image differencing. The forest area dynamics was further studied by analysing the different types of fragmentation through forest fragmentation models. The computed forest fragmentation and landscape metrics show a decline of interior intact forests with a substantial increase in patch forest during 1972-2007.

1. Introduction

Landscape refers to a portion of heterogeneous territory composed of sets of interacting ecosystems and are characterised essentially by its dynamics that are partly governed by human activities. The physical state of the earth's immediate surface in terms of vegetation, soil, water, and human-made structures (e.g. buildings) at any instant of time constitute land cover (LC). Land use (LU) refers to the way humans and their habitat use land resources, usually with assent on the functional role of land for economic activities. LC changes in the recent times have influenced economics, environment, culture, and demography at regional levels. Consequences of LC changes such as forest fragmentation pose serious threats to biodiversity and endanger the sustainability of ecological goods and services. The change in LC and LU types can be obtained from multi-satellite sensor spatio-temporal data using efficient classification algorithms and pattern recognition techniques [1]. The classification algorithms can either be unsupervised or supervised. In the former, no training data is utilised for classification. Instead the classifiers examine the unknown pixels in an image and aggregate them into comparatively well-separated spectral classes based on the natural groupings or clusters. In the latter case, the analyst has training data which is used to train the classifier and also the outcome of the classification is validated with the independently collected test data.

Numerous statistical classification algorithms exist, each one having a genesis behind its evolution. Depending on the nature of the data sources and methodology, multi-source, multi-sensor, multi-temporal, multi-frequency or multi-polarisation data are being used [2-4]. In most of the cases, the algorithms perform well with high degrees of accuracy, however, in an undulating terrain, where there is a large variation in spectral response due to high relief and shadow, the performance of a classifier

deteriorates. Another major problem with these classifiers is their inability to classify data at different measurement scales and units due to invalid assumptions of statistical distributions. Temporal analysis of the spatial data provides an idea of the extent of changes happening in the landscape. LU details derived from temporal remote sensing (RS) data offer potential for assessing the changes in land uses, forest fragmentation and its impact on biodiversity, economics, greenhouse gas emission and hydrology. Spatial LU maps indicate only the location and type of forest, and further analyses are needed to quantify forest fragmentation. Hence, fragmentation of forests was assessed to understand the implication of temporal dynamics on forest habitats. Forest fragmentation is the process whereby a large, contiguous forest is both reduced in area and divided into two or more fragments. The decline in size of the forest and the increasing isolation between the two remnant patches of the forest has been the major cause of declining biodiversity [5]. The primary concern is direct loss of forest area, and all disturbed forests are subject to "edge effects" of one kind or another. Forest fragmentation is of additional concern, insofar as the edge effect is mitigated by the residual spatial pattern [6]. In this context, objectives of this communication is to

1) evaluate the performance of the different classification techniques (for land use analysis).

2) analyse the landscape dynamics using temporal RS data.

3) model the forest fragmentation in the landscape.

2. Materials and Methods

2.1. Data

Survey of India (SOI) toposheets of 1:50000 and 1:250000 scales were digitised to derive base layers. Ground control points (GCPs) for geo-rectification and training data for supervised classification of RS data were collected through field investigations using a hand-held GPS. Google Earth data (http://earth.google.com) were used pre and post classification and also for validation. The RS data used for the study are Landsat MSS (79 m, 4 bands, acquired: November 15, 1972), Landsat TM (30 m, 6 bands, acquired: October 9, 1989), Landsat ETM+ (30 m, bands 1 - 5 and 7, band 8 - Panchromatic of 15 m, acquired: October 15, 2000) and IRS LISS-III (23.5 m, 3 bands, acquired: May 9, 2007). Landsat data were downloaded (from http://glcf.umiacs.umd.edu/data/) and IRS data were procured from National Remote Sensing Centre, Hyderabad, India. Bands were geocorrected with the known GCP's, and projected to geographic latitude-longitude with WGS-84 datum, followed

by masking and cropping of the study area. Landsat data (of 1972) were resampled to 60 m, Landsat TM data of 1989 and IRS LISS III were resampled to 15 m using nearest neighbourhood technique.

Study area: Moolbari watershed is situated in Shimla district, Himachal Pradesh, India as a part of Yamuna river basin and encompasses an area of 13.41 sq. km. from 31.07 - 31.17°N 77.05 - 77.15°E (**Figure 1**). The altitude ranges from 1400 - 2000 m amsl.

The vegetation in Moolbari is of mid-temperate comprising mixed deciduous (up to 1500 m) and sub-tropical pine forest (above 1500 m) in two different altitudinal ranges. There are reserve forests managed by state forest department, insofar cutting of trees is prohibited. However, lopping and collection of fallen wood for household purposes by the villagers are noted.

2.2. Methods

The methods adopted in the analysis involve principal component analysis (PCA) based fusion, Land cover (LC), Land use (LU) analysis, change detection and forest fragmentation analysis.

2.2.1. Image Fusion

This was done using PCA fusion to increase the spatial resolution of multichannel image by introducing an image with a higher resolution. PC analysis was performed separately on the 6 bands of Landsat TM of 1989 (of spatial resolution 15 m) and 4 bands of Landsat MSS data of 1972 (of spatial resolution 60 m). PC1 of Landsat TM 1989 was stretched to have same mean and variance as that of PC1 of Landsat MSS using equation 1 [7].

$$DN_{new\_image} = \frac{\sigma_{ref}}{\sigma_{old}}\left(DN_{old} - \mu_{old}\right) + \mu_{ref} \qquad (1)$$

where DN_{new_image} is the image that has same mean and variance as that of principal component (PC) 1 of Landsat MSS, μ_{ref} and σ_{ref} refers to the mean and standard deviation of PC1 of Landsat MSS. DN_{old}, μ_{old} and σ_{old} represent the digital number, mean and standard deviation of PC1 of Landsat TM (1989).

PC1 of Landsat MSS was replaced with PC1 of higher resolution Landsat TM of 1989 as it contains the information which is common to all bands while the spectral information is unique for each band. PC1 accounts for maximum variance which can maximise the effect of the high resolution data in the fused image. Finally, high-resolution multispectral images were determined by performing the inverse PCA transformation. Similarly, Panchromatic band at 15 m resolution was fused with the 6 bands (at 30 m) of Landsat ETM+ (2000). With this, the RS data corresponding to 4 time periods were at a uniform spatial resolution of 15 m for easy analysis, con-
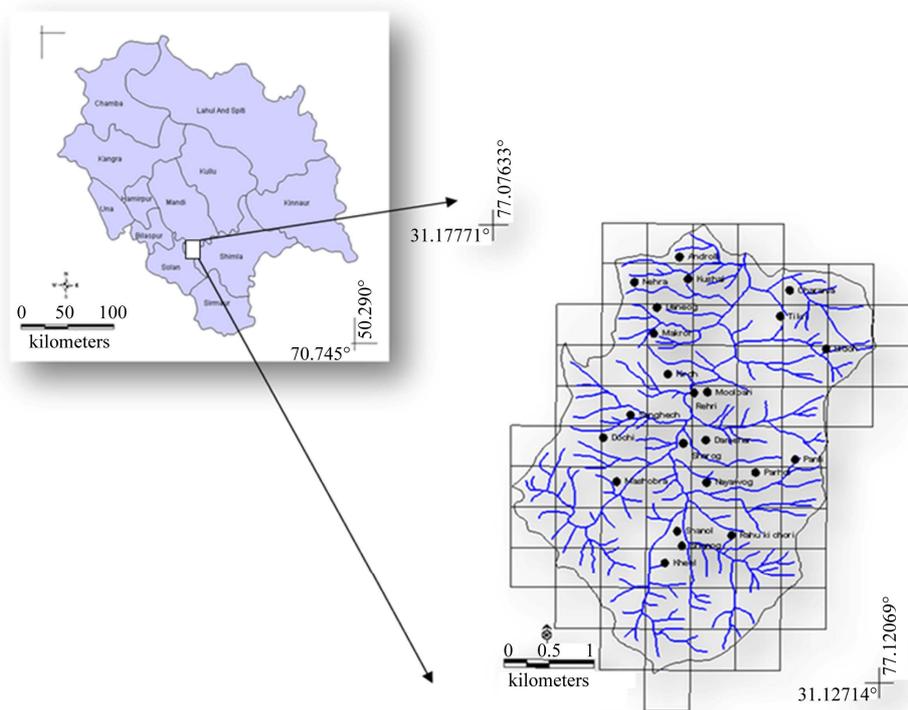
Figure 1. Moolbari watershed.

sistency and multi-date pixel to pixel comparison. These data were used subsequently for LU classification and spatial change analysis.

2.2.2. Land Cover (LC)

NDVI was computed to segregate regions under vegetation, soil and water using NIR and Red bands of temporal data.

2.2.3. LU Classification

The classification techniques evaluated on temporal data (with diverse spatial and spectral resolutions) are: Gaussian Maximum Likelihood Classifier (GMLC), Minimum distance to means, Mahalanobis distance, Parallelepiped and Binary Encoding (BE).

1) GMLC—It quantitatively evaluates both the variance and covariance of the category spectral response patterns when classifying an unknown pixel [8], assuming the distribution of data points to be Gaussian. The distribution of a category response pattern can be completely described by the mean vector and the covariance matrix. The statistical probability of a given pixel value being a member of a particular class are computed. After evaluating the probability in each category, the pixel is assigned to the most likely class (highest probability value).

2) Minimum distance to Means—Here, the mean spectral value in each band for each category is determined

[8,9]. These values comprise the mean vector for each category. A pixel of unknown identity may be classified by computing the distance between the value of the unknown pixel and each of the category means. After computing the distances, the unknown pixel is assigned to the closest class.

3) Mahalanobis distance—When the covariance matrices for all of the classes are identical but otherwise arbitrary [1,10], samples fall in hyperellipsoidal clusters of equal size and shape, the cluster for the ith class being centred about the mean vector μ_i. The optimal decision rule to classify a feature vector x would be to measure the squared Mahalanobis distance $\left(x - \mu_i\right)^t \Sigma^{-1}\left(x - \mu_i\right)$ from x to each of the mean vectors, and assign x to the closest category.

4) Parallelepiped classifier—Parallelepiped classifier [11] is a multidimensional analogy of the box classifier [12]. It allows multi-dimensional boxes that are used for multispectral bands. Each box in the parallelepiped classifier is formed by the maximum (max.) and minimum (min.) values in each training class data in each band. For multispectral bands, the parallelograms will be obtained. The sensitivity or category variance is introduced by considering the range of values in each category training set defined by the highest (max.) and lowest (min.) digital number in each band. An unknown pixel is classified according to the decision region in which it lies [8]. The class signatures come from the analyst defined

training sites. A pixel is classified as a member of a class if and only if all of its band information or signature falls within the corresponding ranges of the bands defined by that class.

5) BE—The most primitive and natural preprocessing of spectral data for qualitative identification is binary (one bit) encoding [13,14]. Hamming distance, which is the binary equivalent of the Euclidean distance, is used as a dissimilarity metric. The vector for an individual spectrum represents a point in hamming space with unit edge in a hypercube. Since only 0 and 1 are assigned to peak intensities, all of the spectral points lie only on the corners (vertices) of the hypercube. Hamming distance between two spectral points is equal to the number of mismatches between the binary encoded data vectors (spectra) being compared and is the same as the result obtained by application of the logical exclusive OR operator (XOR) to the two spectra.

Accuracy assessment of these techniques was done using error matrix and receiver operating characteristic (ROC) curves to choose the best classifier.

2.2.4. LU Change Detection

This is performed by change/no-change recognition followed by boundary delineation on images of multi time periods [15]. Changes across a period of 35 years were analysed through PCA, correspondence analysis (CA) and Normalised Difference Vegetation Indices (NDVI) differencing based change detection.

1) PCA—PCA is effective for change detection [16,17] and is implemented on bi-temporal multispectral images. The major components of the time two image are subtracted from the corresponding components of the time one image to obtain differences related to changes in LU. Changes are detected at the lower-end and higher-end tails of the PC difference image pixels distribution histogram.

2) CA transformation—In CA [18], data table is transformed into a table of the contribution using Pearson chi-square statistic. Pixel (x_{ij}) values are initially converted to proportions (p_{ij}) by dividing each pixel (x_{ij}) value by the sum (x_{++}) of all the pixels in the data set. This threshold in a new dataset of proportions (Q) with the size of (rxc). Row weight p_{i+} is equal to x_{i+}/x_{++}, where x_{i+} is the sum of values in row i. Vector [p_{i+}] is of size (r). Column weight p_{+j} is equal to x_{+j}/x_{++}, where x_{+j} is the sum of values in column j. Vector [p_{+j}] is of size (c). The Pearson chi-square statistic χ^2_p, is a sum of squared χ_{ij} values, computed for every cell ij of the contingency table. q_{ij} values were used instead of χ_i values to form the matrix $\overline{Q}_{r \times c}$ so that $q_{ij} = \chi_{ij}/\sqrt{x_{++}}$ and eigenvalues would be smaller than or equal to 1. Multispectral data are then transformed into the component space using the

matrix of eigenvectors. Image differencing is applied to CA components to perform change detection.

3) NDVI differencing—In NDVI differencing [19,20], areas of change can be identified through the subtraction of the NDVI image of one date from the NDVI image of another date. However, NDVI technique produces limited discriminating abilities in areas less dominated by vegetative ground cover types.

2.2.5. Forest Fragmentation

Forest fragmentation analysis was done to quantify the type of forest in the study area-patch, transitional, edge, perforated, and interior based on the classified images. Additionally, landscape metrics were computed to understand the fragmentation process at a patch and class level. These metrics along with the state of the forest fragmentation index was used to quantify and investigate the fragmentation process.

Forest fragmentation statistics and the total extent of forest and its occurrence as adjacent pixels is computed through fixed-area windows surrounding each forest pixel, which is used to classify the window by the type of fragmentation. The result is stored at the location of the centre pixel. Thus, a pixel value in the derived map refers to between-pixel fragmentation around the corresponding forest location [21]. Forest fragmentation category at pixel level is computed through *Pf* (the ratio of pixels that are forested to the total non-water pixels in the window) and *Pff* (the proportion of all adjacent (cardinal directions only) pixel pairs that include at least one forest pixel, for which both pixels are forested.) Pff estimates the conditional probability that given a pixel of forest, its neighbour is also forest. Based on the knowledge of *Pf* and *Pff* [21], six fragmentation categories: (1) interior, when *Pf* = 1.0; (2) patch, when *Pf* < 0.4; (3) transitional, when 0.4 < *Pf* < 0.6; (4) edge, when *Pf* > 0.6 and *Pf* – *Pff* > 0; (5) perforated, when *Pf* > 0.6 and Pf – *Pff* < 0, and (6) undetermined, when *Pf* > 0.6 and *Pf* = *Pff* are mapped.

Based on these forest fragmentation indices, Total forest proportion (TFP: ratio of area under forests to the total geographical extent excluding water bodies), weighted forest area (WFA) and Forest continuity (FC) are computed. TFP provides a basic assessment of forest cover in a region ranging from 0 to 1. Weighted values for the weighted forest area (WFA) are derived from the median *Pf* value for each fragmentation class as given by Equation (2) below:

$$\begin{aligned}
WFA = \,&(1.0 * \text{interior}) \\
&+ (0.8 * (\text{perforated} + \text{edge} + \text{undetermined})) \quad (2) \\
&+ (0.5 + \text{transitional}) + (0.2 * \text{patch})
\end{aligned}$$

$$FC = \frac{\text{weighted forest area}}{\text{total forest area}}$$
$$* \frac{\text{area of largest interior forest patch}}{\text{total forest area}}$$

(3)

TFP designations are as per Vogelmann (1995) [22] and Wickham *et al.* (1999) [23]. Forest fragmentation become more severe as forest cover decreases from 100 percent towards 80 percent. Between 60 and 80 percent forest cover, the opportunity for re-introduction of forest to connect forest patches is the greatest, and below 60 percent, forest patches become small and more fragmented. The FC regions were evenly split and designated as high forest continuity (above 0.5) or low forest continuity (below 0.5). FC value examines only the forested areas within the analysis region. The rationale is that given two regions of equal forest cover, the one with more interior forest would have a higher weighted area, and thus be less fragmented. To separate further regions based on the level of fragmentation, the weight area ratio is multiplied by the ratio of the largest interior forest patch to total forest area for the region. FC ranges from 0 to 1.

3. Results and Discussion

NDVI was computed with the temporal data of 1972, 1989, 2000 and 2007 for land cover analysis to delineate area under green (agriculture, forest and plantations/or-

chards) and non-green (built up land, waste/barren rock and stones). This shows the reduction of region under vegetation by 5.59% during three decades.

Further analyses of four datasets were done using Iterative Self-Organising Data (ISO data) [24,25] clustering to understand the number of probable classes. It indicated that mapping of the classes could be done accurately, giving an overall good representation of what was observed in the field. Initially 25 clusters were made, and clusters were merged one by one to produce a map with three distinct classes: forest, agriculture and barren land that were the dominant categories in the study area. Signature separability of the LU classes was done using Transformed divergence (TD) matrix and Bhattacharrya (or Jeffries-Mastusuta) distance and spectral graphs (**Figure 2**). Both the TD and Jeffries-Mastusuta measures are real values between 0 and 2, where '0' indicates complete overlap between the signatures of two classes and '2' indicates a complete separation between the two classes. Both measures are monotonically related to classification accuracies. The larger the separability values, the better the final classification results. The possible ranges of separability values are 0.0 to 1.0 (very poor); 1.0 to 1.9 (poor); 1.9 to 2.0 (good). Very poor separability (0.0 to 1.0) indicates that the two signatures are statistically very close to each other [26]. **Figure 2** shows that all the classes are well separable except barren and agriculture in band 4 of Landsat TM/ETM and IRS LISS-III data.
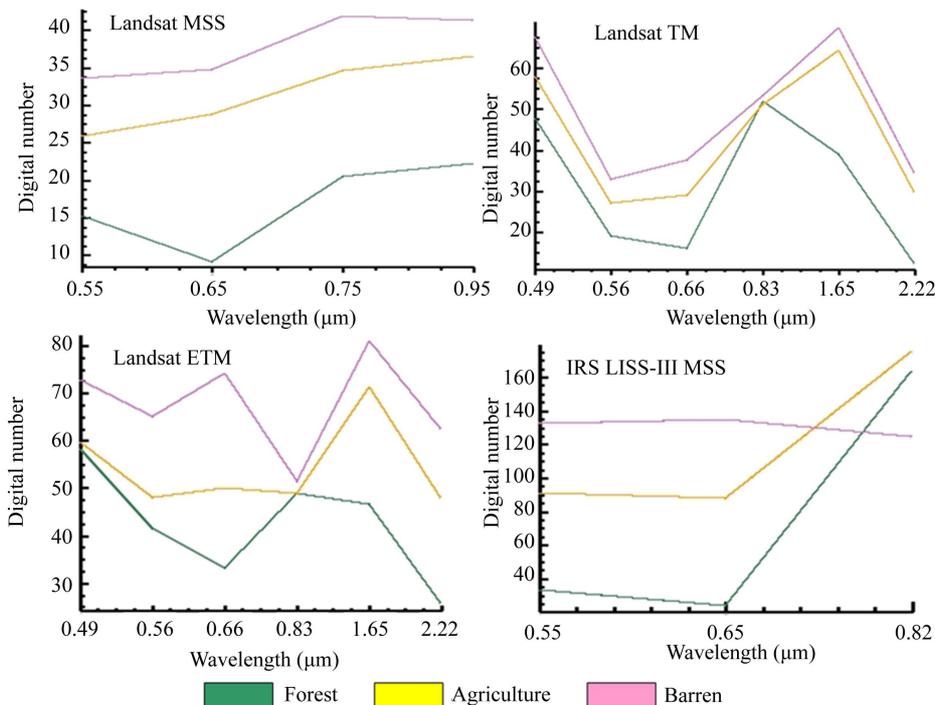

Figure 2. Spectral signature separability for various sensor data.

Supervised classification was performed for land use analysis based on the training data uniformly distributed representing / covering the study area using the five algorithms. GMLC output is shown in **Figure 3**. The error matrix [27] is given in **Table 1** and ROC curves [28] were plotted for each class (**Figure 4**) to assess the accuracy of the classified data.

ROC curve helped in visualising the performance of a classification algorithm as the decision threshold could be varied algorithm-wise for each class. The best possi-

ble classification would yield a point in the upper left corner or coordinate (0,1) of the ROC space, representing 100% sensitivity (all true positives are found) and 100% specificity (no false positives are found). The (0,1) point is also called a *perfect classification*. A completely random guess would give a point along a diagonal line (*line of no-discrimination*) from the left bottom to the top right corners. The diagonal line divides the ROC space in areas of good or bad classification. Points above the diagonal line indicate good classification results, while points
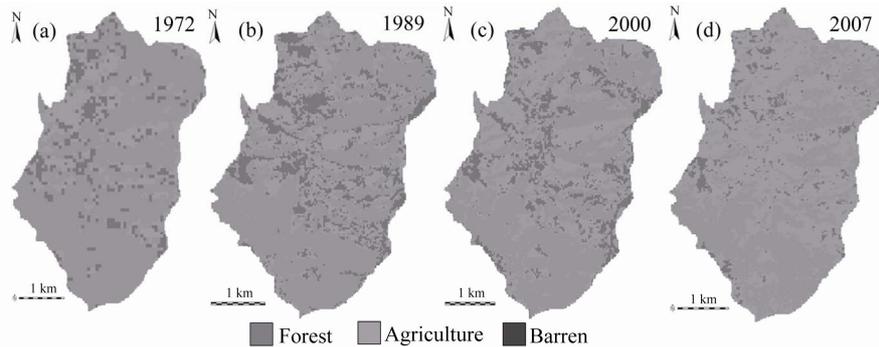

Figure 3. GMLC based LU classification using (a) Landsat MSS, 1972, (b) Landsat TM, 1989, (c) Landsat ETM, 2000 and (d) IRS LISS-III, 2007.
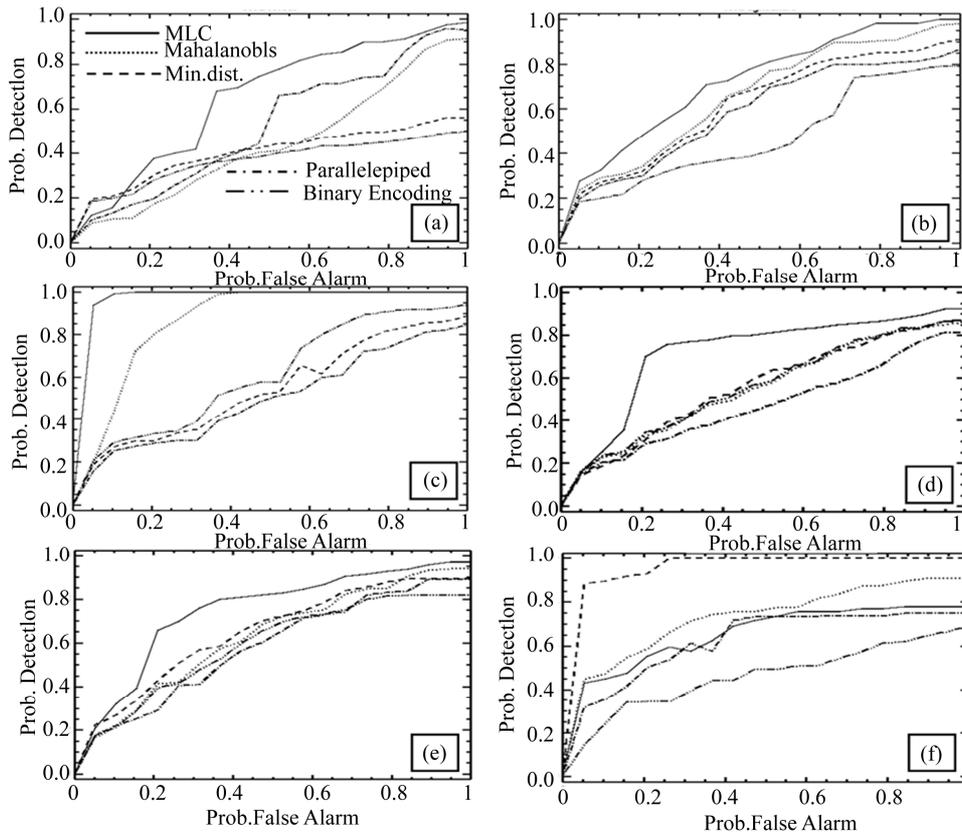

Figure 4. ROC curves for [a] Forest (1972); [b] Agriculture (1972); [c] Barren (1972); [d] Forest (2007); [e] Agriculture (2007); [f] Barren (2007) for the five different classifiers.

Table 1. Overall accuracy and kappa statistics for each classifier (OA - Overall Accuracy).

Algorithm	1972		1989		2000		2007	
	OA	Kappa	OA	Kappa	OA	Kappa	OA	Kappa
GMLC	88.95	0.84	88.52	0.85	80.85	0.76	88.36	0.83
Mahalanobis distance	84.41	0.76	77.78	0.74	80.66	0.77	72.27	0.69
Minimum distance	79.66	0.75	86.33	0.79	76.53	0.59	85.01	0.81
Parallelepiped	82.55	0.74	77.33	0.73	56.70	0.53	76.66	0.72
BE	75.16	0.68	86.00	0.81	61.20	0.56	79.73	0.68

below the line indicate wrong results [29].

There is a good agreement between results obtained from error matrix and ROC curves to the ranking of the performance of the classification algorithms. They indicate that GMLC is the best performing algorithm for different sensor datasets (**Table 2**). This conventional per-pixel, spectral-based classifier constitutes a historically dominant approach to RS-based automated LU and LC derivation [30,31]. In fact, this aids as "benchmark" for evaluating the performance of novel classification algorithms [32].

Results of all these algorithms are valid only for the particular architecture or parameter settings tested although there may be other architectures that offer better performance. Selection of parameters is done based on the training data, evaluation, and test set methodology. Finally, for one particular application, the best way to select a classifier and its operational point is to use the Neyman-Pearson method of selecting the required sensitivity and then maximising the specificity with this constraint (or vice versa). The spectral signature curve for IRS LISS-III shows confusion between barren and agriculture. A similar result was obtained in the Jeffries-Matusita matrix with the separability values of 1.4 (poor separability). This was also observed while performing the clustering on LISS-III data.

The analysis showed GMLC to be better among the five algorithms. However, the successful application of GMLC is dependent upon having delineated correctly the spectral classes in the image data of interest. This is necessary because each class is to be modelled by a normal probability distribution. GMLC can obtain minimum classification error under the assumption that the spectral data of each class is normally distributed. The disadvantage is that it require its' every training set to include at least one more pixel than the number of bands. If a class happens to be multimodal, and this is not resolved, then clearly the modelling cannot be very effective. Mahalanobis distance is similar to any other statistical classifier and uses Mahalanobis distance as a metric. It takes into account errors associated with prediction measurement such as noise, by using the feature covariance matrix to scale features according to their variances. This

classifier performed well on 1972 and 2000 images. Minimum distance to Means is mathematically simple and computationally efficient. However, it has more error of omission and commission. It is insensitive to different degrees of variance in spectral response data. Therefore it should not be used where spectral classes are close to one another in the measurement space and have high variance. Although Parallelepiped algorithm did not perform very well, it is known for its good computational speed. When pixels are within overlapped region of parallelogram, then it may perform unsatisfactorily as pixels will end up unclassified and lead to error of omission. BE did not perform very well for any dataset. However, this technique has been reported useful for high spectral resolution data where high-speed spectral signature matching is required. In order to effectively use this technique for spectral clustering, one must account for spectra which are relatively flat and devoid of absorption features.

Spatial change in LU pattern from 1972 to 2007 is shown in **Table 3**. There is a decline of forest patches (48%) during the last three decades due to increasing agricultural practices. Agricultural area has significantly increased from 264 hectares (1972) to 779 hectares (2007). Barren area has increased by 23% (during 1972 to 2000). Barren land mainly constitutes the rocks, stones, and built ups. However, the proportion of barren land in 2007 is less compared to earlier classified images as some pixels corresponding to barren areas with grass cover showed similar spectral aspects as agriculture, which can be ascertained from **Figure 5**.

Difference of temporal PCs, CA-PC's, NDVI images and bands (rescaled from –1 to 1) showed similar results. To see the change in forest and agriculture, the NIR band of 1972 (T1) and 2007 (T2) were used which have the advantage of highlighting vegetation pixels because of the maximum reflectance by the green plants. The two NIR bands were first normalised by subtracting the image minimum and dividing by the image data range. Normalised temporal maps were then subtracted (T2 – T1) to see the absolute change in pixel values and were then converted to relative difference map with values ranging from –1 to +1 with 0 representing no change, –1

Table 2. Ranking of algorithms based on overall accuracy.

Rank	1972	1989	2000	2007
1	MLC	MLC	MLC	MLC
2	Mahalanobis	Min. dist. To mean	Mahalanobis	Min. dist. To mean
3	Parallelepiped	Binary Encoding	Min. dist. To mean	Binary Encoding
4	Min. dist. To mean	Mahalanobis	Binary Encoding	Parallelepiped
5	Binary Encoding	Parallelepiped	Parallelepiped	Mahalanobis

Table 3. LU change from 1972, 1989, 2000 and 2007.

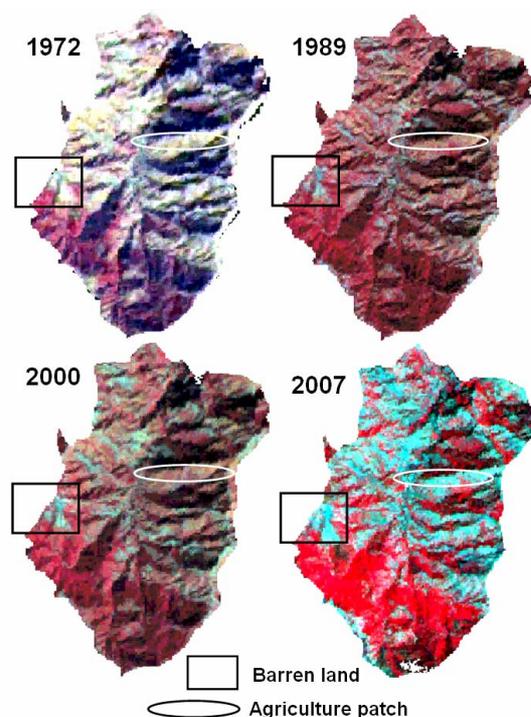| Year	Area	Forest	Agriculture	Barren
1972	**Ha**	925	264	152
	%	68.97	19.67	11.35
1989	**Ha**	706	398	229
	%	52.97	29.84	17.18
2000	**Ha**	591	555	187
	%	44.37	41.63	14.00
2007	**Ha**	474	779	88
	%	35.38	58.08	6.54

Figure 5. FCC of Landsat MSS (1972), Landsat TM (1989), Landsat ETM (2000) and LISS-III (2007). FCC of 2007 shows similar reflectance of barren/stone and agricultural patch leading to confusion between these two classes.

representing negative change and positive values representing increase in the value of the digital number of pixels from 1972 to 2007.

In both the images of the non-standardized PCA, PC1 had the highest information having all bands with unequal variances. CA puts less emphasis on bands that have low polarisation. Higher is the importance given to that band in the calculation of the between-pixel distances if more number of pixels are polarised in a band. First two components of CA explained approximately 99% of the total inertia in both images (**Table 4**). Total inertia is a measure of how much the individual pixel values are spread around the centroid.

Detailed change detection tabulation was done between two classified images of 1972 and 2007. The analysis focuses primarily on the initial state classification changes—that is, for each initial state class (in 1972), it identifies the classes into which those pixels changed in the final state image (in 2007). Changes are reported as pixel counts, area and percentages in **Table 5** that list the *initial state classes in the columns* and the *final state classes in the rows* for the paired initial and final state classes. The rows contain all of the final state classes (2007) which are required for complete accounting of the distribution of pixels that changed classes.

For each initial state class (*i.e.*, each column), the table indicates how these pixels were classified in the final state image. In **Table 5**, 18209 pixels (410.55 ha) initially classified as forest (in 1972) changed into agriculture class in the final state image (2007). 23025 pixels were classified as forest in the initial state image (in 1972). The *Class Total Row* indicates the total number of pixels in each initial state class, (42370 in the Forest column = 23025 + 18209 + 1136, similarly there are 10350 pixels in agriculture and 6759 pixels in barren class) in 1972. The *Class Total Column* indicates the total number of pixels in each final state class (29361 pixels were classified as agriculture in the final state image).

The *Row Total Column* is simply a class-by-class summation of all the final state pixels that fell into the selected initial state classes. Sometimes this may not be the same as the *Class Total Column* (*i.e.* final state class total) because it is not required that all initial state classes be included in the analysis. For example, if there was a fourth class "water" in 1972 and were absent in 2007 classified image or not considered while classification then the *Row Total Column* would not be equal to *Class Total Column* because total number of pixels in any final state class will not be equal to summation of all the final state pixels in that class. The difference in the *Row Total Column* and *Class Total Column* are due to those pixels. However, in the present case, *Row total*

Table 4. Eigen structure of 1972 and 2007 data after PCA and CA transformation.

		Landsat MSS (1972)			IRS LISS-III (2007)		
		Comp1	Comp2	Comp3	Comp1	Comp2	Comp3
PCA	Band 1	0.3175	0.3370	0.8863	−0.3589	0.5657	0.7424
	Band 2	0.5484	0.6973	−0.4616	−0.4747	0.5742	−0.6670
	Band 3	0.7736	−0.632	−0.0366	0.8037	0.5918	−0.0624
	Eigenvalues	168.50	9.3156	0.9892	2.9085	1.5724	0.0291
	Proportion	94.23	5.20	0.57	64.49	34.87	0.64
	Cumulative	94.23	99.43	100	64.49	99.36	100
		Landsat MSS (1972)			IRS LISS–III (2007)		
		Comp1	Comp2	Comp3	Comp1	Comp2	Comp 3
Correspondence Analysis	Band 1	0.5155	0.8569	0.00001	0.6710	0.1153	0.7325
	Band 2	0.6059	−0.365	0.7071	0.6866	0.2762	−0.6725
	Band 3	0.6059	−0.365	−0.7071	0.2799	−0.9541	−0.1061
	Eigenvalues	0.2681	0.0119	−0.0001	0.2595	0.0765	0.0040
	Proportion	95.71	4.25	0.036	76.32	22.5	1.176
	Cumulative	95.71	99.96	100	76.32	98.82	100

Table 5. LU change detection statistics (1972 to 2007).

			Initial State (1972)				
			Forest	**Agriculture**	**Barren**	**Row Total Column**	**Class Total Column**
Final State (2007)	**Forest**	Pixels	**23025**	1924	1797	26766	26766
		Area (ha)	519.13	43.38	40.52	603.03	603.03
		Percent	38.71	3.23	3.02	44.96	44.96
	Agriculture	Pixels	**18209**	6993	4159	**29361**	**29361**
		Area (ha)	410.55	157.66	93.77	661.99	661.99
		Percent	30.61	11.76	6.99	49.36	49.36
	Barren	Pixels	**1136**	1436	803	3375	3375
		Area (ha)	25.61	32.38	18.12	76.09	76.09
		Percent	1.91	2.41	1.35	5.67	5.67
	Class Total Row	Pixels	**42370**	**10350**	**6759**		
		Area (ha)	955.29	233.42	152.39		
		Percent	71.23	17.41	11.36		
	Class Changes Row	Pixels	**19345**	3357	5956		
		Area (ha)	436.16	75.76	134.27		
		Percent	32.52	5.65	10.01		
	Image Difference Row	Pixels	**−15604**	**+19011**	−3348		
		Area (ha)	−352.27	+428.57	−76.3		
		Percent	−26.27	+31.95	−4.32		

Column indicates that there is no unclassified pixel as same numbers of pixels are also reported in the *Class Total Column*.

The *Class Changes Row* indicates the total number of initial state pixel that changed classes. In **Table 5**, the total class change for forest is 19345 pixels. In other words, 19345 pixels that were initially classified as forest changed into final state classes other than forest. To confirm that this is correct, the number of initial forest classified pixels 23025 are subtracted from the forest class total 42370, which is 19345. The *Image Difference Row* is the difference in the total number of equivalently classed pixels in the two images, computed by subtracting the initial state class totals from the final state class totals (*i.e. Class Total Column-Class Total Row*). An image difference that is positive indicates that the class size increased. The table shows that there is a decrease of 15604 pixels (352.27 ha) in forest class and there has been an increase of 19001 pixels (428.57 ha) in agriculture class.

Temporal analysis revealed large scale LC changes in the region. To understand the level of changes, fragmentation analysis was done, which would help in assessing the state of fragmentation and its implications. In this regard, *Pf* and *Pff* in a fixed-area window of 3 × 3 were computed [21] to identify forest fragmentation categories given in **Figure 6** and **Table 6**.

The case of *Pf* = 1 (interior) represents a completely forested window for which *Pff* is also 1. When *Pff* is larger than *Pf*, the implication is that forest is clumped; the probability that an immediate neighbour is also forest is greater than the average probability of forest within the window. Conversely, when *Pff* is smaller than *Pf*, the implication is that whatever is nonforest is clumped. The difference (*Pf-Pff*) characterises a gradient from forest clumping (edge) to nonforest clumping (perforated). When *Pff* = *Pf*, the model cannot distinguish forest or nonforest clumping. To understand the fragmentation process, 10 spatial metrics – Number of patches (NP), Patch density (PD), Total edge (TE), Edge Density (ED), Largest shape index (LSI), Shannon diversity index (SHDI) were calculated at landscape level using Fragstats [33].

Quantitative assessment of the pattern of forest fragmentation and its trends showed that interior forest has declined by 68.81%. Patch forest which was absent in 1972 image has increased up to 12 ha in 2007 and interior forest has decreased from 789 ha in 1972 to 246 ha in 2007. The values of TFP and FC for the temporal data were plotted that specifies six conditions of forest fragmentation in **Figure 7**. The amount of forest and continuity were high in 1972 and declined in 2007.
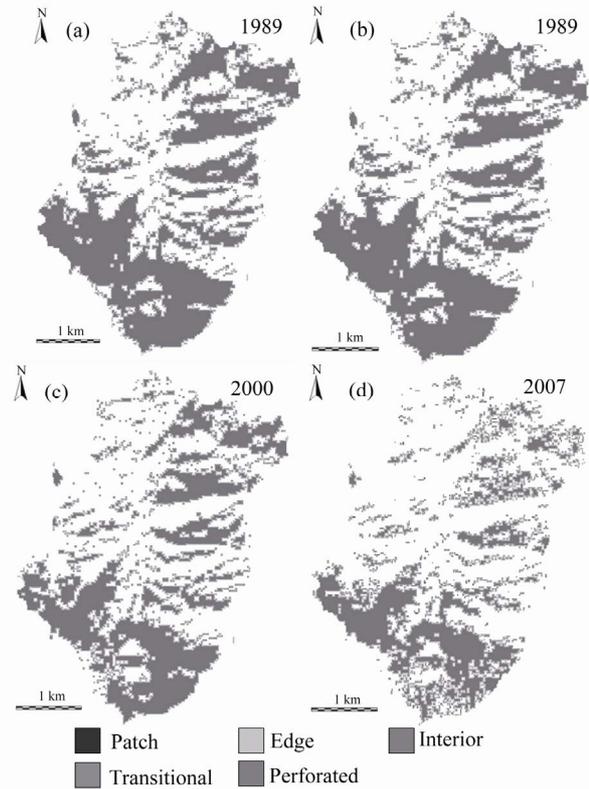
Forest in Moolbari watershed was more contiguous

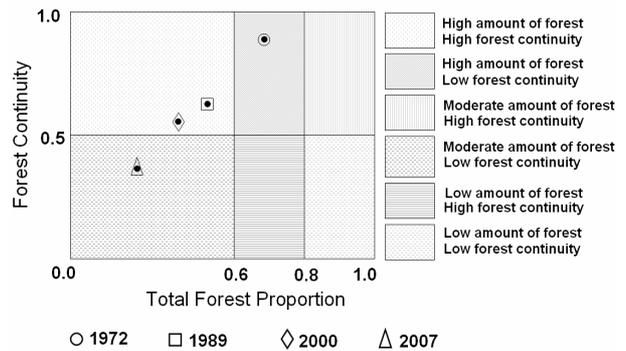**Figure 6. Forest fragmentation map (a) 1972, (b) 1989, (c) 2000, (d) 2007.**

Figure 7. Six forest fragmentation conditions based on the values for Total Forest Proportion and Forest calculated for a region.

earlier (in 1972), with less number of patches than that of 2007. There was a single contiguous patch of forest, which is now more fragmented with interspersion of agriculture land and reduced area (925 ha in 1972 to 474 ha) in 2007. Individually, the largest patch in 1972 was 907 ha, while in 2007, the largest patch is 273 ha. Number of patches and patch density, which are the direct measure of fragmentation effect also increased over years. **Table 7** details the fragmentation metrics calculated at landscape level.

Table 6. Forest fragmentation types details.

	1972		1989		2000		2007	
	ha	%	ha	%	ha	%	ha	%
Interior	788.88	87.42	508.87	73.41	320.65	65.02	246.00	52.61
Perforated	75.60	8.38	62.68	9.04	66.29	11.32	45.48	9.72
Edge	28.63	3.17	85.68	12.36	91.54	15.64	110.50	23.63
Transitional	9.29	1.03	35.75	5.16	46.63	7.96	53.35	11.41
Patch	0.00	0.00	0.22	0.03	0.32	0.05	12.31	2.63
Total	902.40	100	693.21	100	385.42	100	467.63	100

Table 7. Forest fragmentation indices for 1972 to 2007.

Index →	NP	PD	TE	ED	LSI	SHDI
1972	41	1.75	57206.51	24.43	3.46	0.14
1989	95	4.06	78993.03	33.74	4.58	1.48
2000	152	6.49	86560.50	36.97	4.97	2.00
2007	212	9.05	100043.80	42.73	5.67	2.10

From this analysis, it is clear that Moolbari watershed in the ecologically fragile Himalaya is under the severe influence of forest fragmentation, necessitating immediate interventions involving integrated watershed management strategies. The results highlight higher anthropogenic fragmentation in the watershed closer to villages than remote areas.

4. Conclusions

LU classification algorithms were reviewed to assess the best classifier in an undulating terrain. Error matrix along with ROC curves provided a richer measure of classification performance showing that GMLC is superior with overall accuracy of 89% (1972 and 1989), 81% (2000) and 88% (2007). The study showed reduction of region under vegetation by 5.59% during 35 years. Change detection methods revealed a declining trend of forest patches (48%) during the last three decades due to increasing agricultural practices which have significantly increased from 264 ha (1972) to 779 ha (2007). Barren area has increased by 23% (during 1972 to 2000).

Forest fragmentation model showed that interior forest has declined by 68.81% (from 789 ha in 1972 to 246 ha in 2007). Patch forest which was absent in 1972 image has increased up to 12 ha in 2007. Forested area is negatively correlated to all the indices, hinting that decreased forest area has more fragmented patches. Patches come from many sources, ranging from our abilities to visualise and delineate what they represent, to their usage as conceptual units and patch dynamics models and to societal biases such as land ownership and anthropogenic activities. The analysis places patches into perspective as one identifiable element along a continuum of forest fragmentation, and suggest that more attention should be given for the conservation of interior forests and restoration of patch forests for the sustainability of watershed, livelihood and food security.

5. Acknowledgements

6. References

[1] R. O. Duda, P. E. Hart and D. G. Stork, "Pattern Classification," 2nd Edition, A Wiley-Interscience Publication, Hoboken, 2000.

[2] M. K. Arora and S. Mathur, "Multi-Source Classification Using Artificial Neural Network in Rugged Terrain," *Geocarto International*, Vol. 16, No. 3, 2001, pp. 37-44. doi:10.1080/10106040108542202

[3] R. M. Rao and M. K. Arora, "Overview of Image Processing," In: P. K. Varshney and M. K. Arora, Eds., *Advanced Image Processing Techniques for Remotely Sensed Hyperspectral Data*, Springer-Verlag, Berlin, 2004, pp. 51-85.

[4] G. Simone, A. Farina, F. C. Morabito, S. B. Serpico and L. Bruzzone, "Image Fusion Techniques for Remote Sensing Applications," *Information Fusion*, Vol. 3, No. 1, 2002, pp. 3-15. doi:10.1016/S1566-2535(01)00056-2

[5] J. D. Hurd, E. H. Wilson, S. G. Lammey and D. L. Civco,

"Characterization of Forest Fragmentation and Urban Sprawl Using Time Sequential Landsat Imagery," *ASPRS* 2001 *Annual Convention*, St. Louis, 23-27 April 2001.

[6] M. G. Turner, "Landscape Ecology: The Effect of Pattern on Process," *Annual Review of Ecology and Systematics*, Vol. 20, 1989, pp. 171-197. doi:10.1109/TGRS.2005.846874

[7] Z. Wang, D. Ziou, C. Armenakis, D. Li and Q. Li, "A Comparative Analysis of Image Fusion Methods," *IEEE Transactions on Geoscience and Remote Sensing*, Vol. 43, No. 6, 2005, pp. 1391-1402. doi:10.1109/TGRS.2005.846874

[8] T. M. Lillesand and R. W. Kiefer, "Remote Sensing and Image Interpretation," 4th Edition, John Wiley and Sons, New York, 2002.

[9] M. E. Hodgson, "Reducing the Computational Requirements of the Minimum-Distance Classifier," *Remote Sensing of Environment*, Vol. 25, No. 1, 1998, pp. 117-128. doi:10.1016/0034-4257(88)90045-4

[10] M. Wölfel and H. K. Ekenel, "Feature Weighted Mahalanobis Distance: Improved Robustness for Gaussian Classifiers," 13*th European Signal Processing Conference*, September 2005, Turkey. http://www.eurasip.org/Proceedings/Eusipco/Eusipco2005/defevent/papers/cr1853.pdf.

[11] C.-C. Hung and B.-C. Kuo, "Multispectral Image Classification Using Rough Set Theory and the Comparison with Parallelepiped Classifier," *IEEE International Geoscience and Remote Sensing Symposium*, 6-11 July 2008, Boston, pp. 2052-2055.

[12] R. A. Schowengerdt, "Remote Sensing: Models and Methods for Image Processing," 2nd Edition, Academic Press, San Diego, 1997.

[13] A. S. Mazer, M. Martin, M. Lee and J. E. Solomon, "Image Processing Software for Imaging Spectrometry Data Analysis," *Remote Sensing of Environment*, Vol. 24, No. 1, 1988, pp. 201-210. doi:10.1016/0034-4257(88)90012-0

[14] D. R. Scott, "Effects of Binary Encoding on Pattern Recognition and Library Matching of Spectral Data," *Chemometrics and Intelligent Laboratory Systems*, Vol. 4, No. 1, 1998, pp. 47-63. doi:10.1016/0169-7439(88)80012-1

[15] D. Lu, P. Mausel, E. Brondizio and E. Moran, "Change Detection Techniques," *International Journal of Remote Sensing*, Vol. 25, No. 12, 2004, pp. 2365-2407. doi:10.1080/0143116031000139863

[16] T. Fung and E. LeDrew, "Application of Principal Component Analysis for Change Detection," *Photogrammetric Engineering and Remote Sensing*, Vol. 53, No. 12, 1987, pp. 1649-1658.

[17] R. D. Macleod and R. G. Congalton, "A Quantitative Comparison of Change-Detection Algorithms for Monitoring Eelgrass from Remotely Sensed Data," *Photogrammetric Engineering and Remote Sensing*, Vol. 64, No. 3, 1998, pp. 207-216.

[18] H. I. Cakir, K. Khorram, S. A. C. Nelson, "Correspondence Analysis for Detecting Land Cover Change," *Remote Sensing of Environment*, Vol. 102, No. 3-4, 2006,

pp. 306-317. doi:10.1016/j.rse.2006.02.023

[19] J. G. Lyon, D. Yuan, R. S. Lunetta and C. D. Elvidge, "A Change Detection Experiment Using Vegetation Indices," *Photogrammetric Engineering and Remote Sensing*, Vol. 64, No. 2, 1998, pp. 143-150.

[20] J. R. Jensen, "Introductory Digital Image Processing: A Remote Sensing Perspective," Prentice-Hall, Upper Saddle River, 2004, pp. 467-494.

[21] K. J. Riitters, R. O' Neill, J. D. Wickham, B. Jones and E. Smith, "Global-Scale Patterns of Forest Fragmentation," *Conservation Ecology*, Vol. 4, No. 2, 2000.

[22] J. E. Vogelmann, "Assessment of Forest Fragmentation in Southern New England Using Remote Sensing and Geographic Information System Technology," *Conservation Biology*, Vol. 9, No. 2, pp. 439-449. doi:10.1046/j.1523-1739.1995.9020439.x

[23] J. D. Wickham, K. B. Jones, K. H. Ritters, T. G. Wade and R. V. O'Neill, "Transition in Forest Fragmentation: Implications for Restoration Opportunities at Regional Scales," *Landscape Ecology*, Vol. 14, No. 2, 1999, pp. 137-145. doi:10.1023/A:1008026129712

[24] A. K. Jain and R. C. Dubes, "Algorithms for Clustering Data," Prentice Hall, Englewood Cliffs, 1988.

[25] PCI Geomatics Corporation, ISOCLUS-Isodata Clustering Program. http://www. pcigeomatics.com/cgi-bin/pcihlp/ISOCLUS

[26] J. A. Richards, "Remote Sensing Digital Image Analysis," Springer-Verlag, Berlin, 1986, pp. 206-225.

[27] J. B. Campbell, "Introduction to Remote Sensing," Taylor and Francis, New York, 2002.

[28] T. Fawcett, "An Introduction to ROC Analysis," *Pattern Recognition Letters*, Vol. 27, No. 8, 2006, pp. 861-874. doi:10.1016/j.patrec.2005.10.010

[29] A. P. Bradley, "The Use of the Area under the ROC Curve in the Evaluation of Machine Learning Algorithms," *Pattern Recognition,* Vol. 30, No. 7, 1997, pp. 1145-1159. doi:10.1016/S0031-3203(96)00142-2

[30] J. Gao, H. F. Chen, Y. Zhang and Y. Zha, "Knowledge-Based Approaches to Accurate Mapping of Mangroves from Satellite Data," *Photogrammetric Engineering & Remote Sensing*, Vol. 70, No. 12, 2004, pp. 1241-1248.

[31] D. B. Hester, H. I. Cakir, S. A. C. Nelson and S. Khorram, "Per-pixel Classification of High Spatial Resolution Satellite Imagery for Urban Land-cover Mapping," *Photogrammetric Engineering & Remote Sensing*, Vol. 74, No. 4, 2008, pp. 463-471.

[32] M. Song, D. L. Civco and J. D. Hurd, "A Competitive Pixel-Object Approach for Land Cover Classification," *International Journal of Remote Sensing*, Vol. 26, No. 22, 2005, pp. 4981-4997. doi:10.1080/01431160500213912

[33] K. McGarigal, S. A. Cushman, M. C. Neel and E. Ene, "FRAGSTATS: Spatial Pattern Analysis Program for Categorical Maps," 2002. http://www.umass.edu/landeco/research/fragstats/fragstats.html